Dynamics of Photoinduced Cell Plasma Membrane Injury

William P. Thorpe,* Mehmet Toner,‡ Robert M. Ezzell,‡ Ronald G. Tompkins,‡ and Martin L. Yarmush*‡
*Department of Chemical and Biochemical Engineering, Rutgers University, Piscataway, New Jersey 08855, and ‡Surgical Services, Massachusetts General Hospital, and Shriners Burns Institute, Boston, Massachusetts 02114 USA

ABSTRACT We have developed a video microscopy system designed for real-time measurement of single cell damage during photolysis under well defined physicochemical and photophysical conditions. Melanoma cells cultured in vitro were treated with the photosensitizer (PS), tin chlorin e6 (SnCe6) or immunoconjugate (SnCe6 conjugated to a anti-ICAM monoclonal antibody), and illuminated with a 10 mW He/Ne laser at a 630 nm wavelength. Cell membrane integrity was assessed using the vital dye calcein-AM. In experiments in which the laser power density and PS concentration were varied, it was determined that the time lag before cell rupture was inversely proportional to the estimated singlet oxygen flux to the cell surface. Microscopic examination of the lytic event indicated that photo-induced lysis was caused by a point rupture of the plasma membrane. The on-line nature of this microscopy system offers an opportunity to monitor the dynamics of the cell damage process and to gain insights into the mechanism governing photolytic cell injury processes.

INTRODUCTION

Photodynamic therapy (PDT) involves cell killing through the generation of phototoxins. These phototoxins are liberated by activation of a photosensitizer (PS) which have been taken up by a particular tissue. Antibody targeted photolysis (ATPL) enhances the localization of PS (and therefore phototoxin) by use of a cell specific monoclonal antibody (MAb) as a carrier for the PS (Jiang et al., 1991; Oseroff et al., 1986; Rakestraw et al., 1992). The primary mode of action of both PDT and ATPL is oxidative damage of cellular structures leading to cell death. Most commonly, the clinical targets in PDT or potential ATPL treatments are certain types of neoplastic conditions (e.g., bladder, esophagus, skin) (Dougherty, 1993; Yarmush et al., 1993).

The photoinduced cell injury process is initiated by activation of a PS by light in the presence of molecular oxygen resulting in the generation of a phototoxin by either a type I (generating free radicals) or type II (generating singlet oxygen) process (Hartman et al., 1988; Gollnick, 1968). Investigators have focused upon various aspects of this process including identification and characterization of phototoxins generated by light activation of various PSs (Brault et al., 1988), identification of cellular substrate targets (Comporti, 1989; Fingar et al., 1992; Girotti, 1990), identification and quantification of photo-oxidative products (Girotti, 1979), and correlation of PDT parameters such as light dose levels (J cm^{-2}) and PS concentration with cell death (Matthews et al., 1989; Potter et al., 1987). As a result of these studies, several general observations may be made about the effects of PDT on targeted cells. It has been shown that PDT-induced cell death correlates with increasing PS levels, light dose, and in general, with overall phototoxin dose delivered to target cells (Matthews et al., 1989; Rakestraw et al., 1992). Photodamage specifically directed to the cell plasma membranes results in cell lysis and increased membrane permeability to ions (e.g., Ca^{2+}, Na^{2+}) (Deziel, 1981; Girotti et al., 1983). Furthermore, cell lysis resulting from photodamage is chiefly mediated by peroxidation of the plasma membrane lipids (Girotti and Deziel, 1983), whereas the increases in membrane permeability to ions is chiefly mediated by direct photodamage of plasma membrane proteins (Girotti and Deziel, 1983). Finally, a significant lag period exists during light irradiation in which the plasma membranes are stable before cell lysis (Deziel, 1981; Girotti and Deziel, 1983).

While PDT effects on targeted cells and cell organelles have been well studied (Gomer, 1991), this information has been acquired primarily with assays involving large cell populations. Little is known about the process of photoinduced cell lysis at the single cell level. Single cell studies that both quantify and control the relevant photophysical and physicochemical parameters in time-dependent photolysis experiments have yet to be performed. Such studies could aid in the development of a better understanding of the changes occurring in the cell plasma membrane during photodamage, which could lead to an improved understanding of the fundamental processes operative during photoinduced cellular damage. Additionally, new insights could be gained about oxidative cell membrane damage for processes other than PDT.

In this study, a quantitative microscopy system was utilized to visualize and analyze the dynamics of photoinduced cell damage. Membrane damage to cells subjected to either targeted or non-targeted PSs was assessed using the plasma membrane integrity probe, calcein-AM. With this system, we have shown: 1) cell lysis is due to a point rupture of the plasma membrane; 2) the time delay preceding the onset of rupture varies inversely to the activating light dose, concentration of PS, and estimated singlet oxygen flux to the surface of the cell; and 3) the kinetics of the dye leakage at the time

Received for publication 28 December 1994 and in final form 23 February 1995.

Address reprint requests to Dr. Martin Yarmush, Department of Chemical and Biochemical Engineering, Rutgers University, Piscataway, NJ 08855. Tel: 908-445-5513; Fax: 908-932-5516.

0006-3495/95/05/2198/09 $2.00

of rupture are independent of singlet oxygen flux levels. These findings will hopefully serve as the basis for a more detailed, comprehensive picture of photoinduced membrane disruption.

MATERIALS AND METHODS

Cells and media

Human malignant melanoma (M21) cells were used as the model system in which the effects of photo-induced membrane damage were examined. These adherent cells were cultured in tissue culture flasks (Falcon, Becton/Dickinson, Franklin Lakes, NJ) with minimum essential media (MEM), (GIBCO, Grand Island, NY) supplemented with 10% fetal bovine serum (GIBCO), 200 mM L-glutamine (Sigma Chemicals, St. Louis, MO) and grown at 37°C in a 5% CO_2 atmosphere. Dulbecco's phosphate buffered saline (DPBS) (GIBCO) and 1% trypsin/EDTA (Sigma) were used as washing and cell removal media, respectively.

Chemicals and biochemicals

Calcein acetoxymethyl ester (calcein-AM, Molecular Probes, Eugene, OR) was the fluorescent cell membrane integrity probe used in these studies. Calcein-AM readily diffuses through cellular plasma membranes and enters the cell cytosol. Endogenous esterases present in viable cells irreversibly cleave the ester moieties in calcein-AM leaving the resultant calcein highly charged (approximately −4) and fluorescent (λ_{exc} ~495 nm, λ_{emm} ~535 nm). Due to both size and charge, calcein does not permeate through the cell membrane and quickly accumulates inside viable cells.

For both the targeted (ATPL) and non-targeted photolysis studies, tin chlorin e6 monoethylenediamine (SnCe6) with triethanolamine axial ligands (coordinated to the Sn) was used as the photosensitizing agent. For ATPL, the SnCe6 was covalently linked to the carbohydrate moiety of a monoclonal antibody (MAb) Fc segment according to the procedure of Lu et al. (1992). The MAb used for ATPL was an anti-intracellular adhesion molecule antibody (α-ICAM, a kind gift from Boehringer Mannheim to Dr. Alan Fishman) that binds to cell surface antigens expressed on the M21 cells. Both ATPL and non-targeted studies were performed by diluting appropriate stock solutions of immunoconjugate, or free SnCe6 in DPBS.

Laser microscopy system

The video microscopy system (Fig. 1) consisted of a Zeiss Axiovert 10 inverted microscope (Zeiss, Thornwood, NY) equipped with a temperature and atmosphere controlled stage, a low light silicon intensified transmittance (SIT) camera and a Nuvicon camera (Hamamatsu, Japan), and a 10-mW He/Ne laser (Aerotech, Pittsburgh, PA). The fluorescence excitation source was a 100-W mercury (Hg) lamp. Light from the Hg source was modified by passage through a fluorescence filter cube set consisting of an excitation filter (450–490 nm) and a dichroic mirror at 510 nm. The SIT camera was used to capture low intensity epifluorescence, while the Nuvicon camera was used to capture transmitted light using Normarsky differential interference contrast (DIC) optics. The video image was then digitized using Image/1 software (Universal Imaging Inc., West Chester, PA) installed on a 486/66 MHz PC. Images were analyzed continuously in real time or logged to storage media (either optical or magnetic disc) for later analysis.

Cell photolysis experiments utilized a 10-mW laser (λ = 630 nm) that was introduced to the optical pathway by a fiber optic cable terminating at a dual light housing (Fig. 1). The dual light house enabled switching from transmitted light (tungsten source) to laser irradiation by a mirror toggle. Laser light was directed through the microscope condenser to the M21 cells on the imaging stage and the laser spot area was controlled by adjusting the condenser diaphragm or by the insertion of custom built pinholes. By adjusting the diaphragm or pinhole in this manner, target areas could be varied from ~5 to 500,000 μm^2. Laser power was measured using a portable digital power meter and Si detector (Newport, Fountain Valley, CA). Power densities were obtained by dividing absolute power by the area of the laser spot.

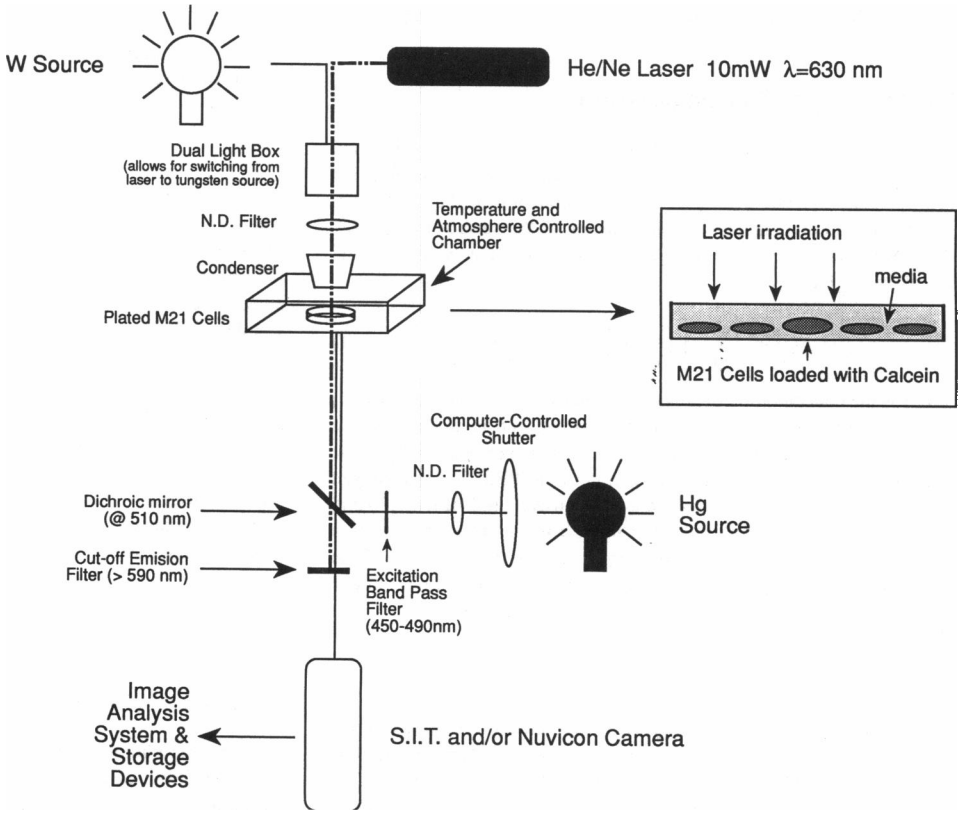

FIGURE 1 Experimental microscopy system equipped with a laser to quantify photodamage to M21 cells.

Local variances in laser intensities due to mode propagation in the fiber optic cable were eliminated by employing a custom built mode mixer. To avoid accidental eye or camera exposure to potentially damaging laser light, an emission filter was built into the filter cube assembly (containing the excitation filter and dichroic mirror) to cut off wavelengths above 590 nm. Photobleaching of calcein by the Hg light was virtually eliminated by combined use of a computer-controlled shuttering system (reducing Hg excitation exposure duration) and neutral density filters (reducing Hg excitation intensity). A Zeiss environmental inverted microscope chamber was used to maintain the cell cultures at 37°C and 5% CO_2 during the photolysis experiments.

Photolysis studies

M21 cells were plated on 12 × 12 mm glass coverslips or 33-mm Petri dishes at a density of 5000 cells cm^{-2} 12 h before use to allow time for the cells to attach and spread but not to divide. Before irradiation with the laser, calcein-AM stock solution (~600 μM) was added to the cells at 1:500 dilution and after 20 min, the cells were rinsed three times with DPBS. For targeted photolysis experiments, a 10 nM solution of immunoconjugate (in DPBS supplemented with Ca^{2+} and Mg^{2+} to maintain cell attachment) was added to the cells. For non-targeted photolysis experiments, increasing concentrations (1, 5, 10, 25 μM) of SnCe6 (in DPBS supplemented with Ca^{2+} and Mg^{2+}) were added to the cells. The cells subjected to PS or immunoconjugate were then placed on the heated microscope stage and allowed to incubate for 5 min before starting an experiment. The targeted cells were irradiated with the laser while the loaded calcein dye was excited by the Hg source. Neutral density filters were used to vary the power density from 50 mW cm^{-2} to 400 mW cm^{-2}. Once an experiment was begun, images were acquired at 2-, 5-, or 10-s intervals.

Incubation times were kept short to confine the damage to the plasma membrane of the cell. In the case of PS alone, SnCe6 was not allowed to incubate with cells for more than 5 min before irradiation. For experiments which utilized immunoconjugates, incubation times were also kept to less than 5 min before irradiation. Internalization was not of concern in these experiments based upon a recent study which showed minimal internalization of an anti-human ICAM-1 antibody on human endothelial cells (<0.1% of bound radiolabeled MAb per minute) (von Asmuth et al., 1992).

Singlet oxygen flux calculation

The flux of singlet oxygen to the surface of M21 cells (N_Δ) was calculated using a model developed by Rakestraw (Rakestraw, 1989). This model is based upon the kinetics of singlet oxygen production in the media surrounding the cell and singlet oxygen diffusion to the surface of the M21 cells. The concentration of singlet oxygen in the immediate vicinity of the cell surface is given by:

$$\Delta(z) = \frac{\phi_\Delta P I \sigma}{hc}\left[\left(\frac{1}{k_d} + \frac{\delta^2}{2D}\right)\frac{z}{\delta} - \frac{z^2}{2D}\right] \quad (1)$$

where Δ is the concentration of singlet oxygen as a function of distance (z) above the cell surface, D is the diffusivity of oxygen in water, P is the concentration of PS in the media, I is the laser power density, k_d is the collective rate constant for singlet oxygen decay in PBS, ϕ_Δ is the singlet oxygen quantum yield for SnCe6 irradiated at a wavelength of λ = 630 nm, h is Planck's constant, c is the speed of light, σ is the molar cross-section for absorbance of SnCe6 at λ = 630 nm, and δ is the thickness of the photodynamic boundary layer above the cell surface. The flux of singlet oxygen at the surface of the cell may be calculated by:

$$N_\Delta = \frac{\phi_\Delta P I \sigma}{hc}\left[\frac{2D + k_d\delta^2}{2k_d\delta}\right] \quad (2)$$

where the gradient of the singlet oxygen is evaluated at the surface of the cell (i.e., $z = 0$). ϕ_Δ for SnCe6 was measured independently to be 0.82 (Rakestraw et al., 1992). D was taken as 3×10^{-5} cm^2 s^{-1} (Lindig et al., 1981), σ was evaluated independently to be 2×10^{-16} cm^2 (Rakestraw et al., 1992), and k_d has been evaluated for Δ in PBS as 2×10^5 s^{-1} (Rakestraw et al., 1992). The value of δ will depend upon the distance a singlet oxygen molecule can diffuse before 1) reacting with a substrate, 2) encountering a quenching agent, or 3) decaying from a variety of radiative and non-radiative processes. In PBS, the lifetime of singlet oxygen is approximately 3 μs (Rodgers et al., 1982). This lifetime corresponds to a "diffusional distance" of ~100 nm. Therefore, for the purposes of this analysis, in which we are interested in analyzing the functional relationships between singlet oxygen flux and dynamic photolysis events, we have evaluated singlet oxygen flux based upon a photodynamic boundary zone of 100 nm.

Measurement of the rupture time constant

An exponential decrease in fluorescence intensity was noted upon the onset of rupture which represented leakage of dye from the ruptured cell. The leakage data from individual cells was fit to the following relation:

$$I_n = \alpha \exp(-t/\tau_L) \quad (3)$$

in which I_n is the normalized cell fluorescence at time t, α is an arbitrary constant, and τ_L is the time constant governing the dye leakage from ruptured cells. τ_L was obtained by regression using a least squares method. The time period during which rupture data was analyzed spanned the onset of rupture to a time point at which cellular fluorescence intensity had reached a minimum.

Estimation of rupture lesion size

An estimate of the rupture lesion dimension was obtained using a mass balance for calcein leakage out of a M21 cell at the time of rupture given by:

$$V\frac{dC}{dt} = j_p S_T p \quad (4)$$

where V is the volume of the cell, C is the calcein concentration inside the cell, j_p is the flux of calcein out of the cell due to passive diffusion (through the rupture lesion), S_T is the cell surface area, p ($= S_h/S_T$) is the porosity of the cell membrane, and S_h is the surface area of the lesion (assumed to be circular for simplicity).

The flux of calcein across the cell membrane by passive diffusion is given by:

$$j_p = -D\frac{\Delta C}{d} = -D\frac{C_i}{d} \quad (5)$$

where D is the diffusivity of calcein in the cytosol, and d is the thickness of the plasma membrane. ΔC is the calcein concentration difference between the intracellular (C_i) and extracellular environment, which reduces to C_i since the concentration of calcein outside the cell is ~0 (due to dilution). Combining Eqs. 4–7 and integrating yields:

$$C_i(t) = C_{i_0} \exp(t/\tau_L) \quad (6)$$

where τ_L(= Vd/DS_h) is the time constant for calcein leakage during cell rupture, and C_{io} is the bulk intracellular calcein concentration just before rupture. Assuming the relative concentration of calcein is proportional to the bulk fluorescence intensity levels within the cell (i.e., $C_i/C_{io} \sim I/I_0$), then the value determined for τ_L experimentally may be used to determined S_h, the rupture lesion size, or:

$$S_h = \frac{Vd}{D\tau_L} \quad (7)$$

Data analysis and statistics

For dynamic photolysis measurements, the background fluorescence was subtracted from each cells fluorescence intensity to obtain the actual intracellular calcein fluorescence. Each acquired image (an average of 8

frames) was then normalized with respect to the fluorescence intensity at time 0. Error bars in Fig. 4 and 5 represent the standard deviation. Data points in Fig. 4 represent the mean value of τ_D from cells in multiple experiments (~15 cells per experiment). Total number of cells per data point varied from 40 to 400.

RESULTS

The objective of this study was to evaluate the dynamic response of single cells to photodamage under well controlled experimental conditions. Specifically, our studies focused upon observing changes in plasma membrane integrity of M21 cells during the photodamage process. The integrity of the cell membrane was assessed dynamically by measuring the intensity of calcein fluorescence inside cells at discrete time points during laser irradiation. Changes in cell membrane integrity were correlated with experimental parameters of photodamage (laser power density and PS concentration) in order to gain a better understanding of the dominant processes occurring during photolysis. Moreover, experiments were performed to evaluate the efficiency of targeted (i.e., ATPL) photolysis compared to non-targeted (i.e., PDT) photolysis.

In the first series of experiments, the effect of varying concentration of SnCe6 on plasma membrane integrity of M21 cells was investigated at a constant laser power density of 150 mW cm^{-2}. M21 cells loaded with calcein were exposed to a known concentration of free SnCe6 for 5 min at 37°C before irradiation from above with the laser (Fig. 1). Micrographs depicting dye leakage from M21 cells surrounded by 25 μM SnCe6/PBS solution as a function of time during laser irradiation are shown in Fig. 2. Fig. 3 shows the normalized intracellular intensity of calcein dye during laser irradiation. As can be seen from this figure, after a lag period (τ_D) of several hundred seconds (during which time <5% of dye loss occurred) there was a sudden and nearly complete loss of dye from the irradiated cell. Controls (which included laser irradiation without the PS, PS without laser irradiation, and neither laser irradiation nor PS) did not show any significant dye loss over the entire observation period. The values of the lag period, τ_D, were analyzed as a function of the incident power density levels and PS concentrations in a series of 24 experiments in which between 10 to 30 cells/experiment were irradiated. The results of these experiments are summarized in Fig. 4A and 4B. τ_D varied inversely with both the power density level and PS concentration over a range of 4 to 380 mW cm^{-2} and 1 to 25 μM SnCe6, respectively.

To determine whether τ_D could be correlated to singlet oxygen generation, a simple kinetic/diffusional model was employed to convert the experimental parameters (i.e., Fig. 4, *A* and *B*) to a estimated singlet oxygen flux (N_Δ). Moreover, additional experiments were performed to investigate a wider range of singlet oxygen flux conditions. These additional flux conditions were achieved by varying power density between 0.50 and 300 mW cm^{-2} and SnCe6 concentrations between 1 to 25 μM. When τ_D was plotted against the reciprocal of estimated values of N_Δ, a linear relation was obtained (Fig. 5). This relationship appeared constant for a wide range of experimental conditions in which the estimated singlet oxygen flux varied from 3.6×10^{15} to 9.4×10^{17} molecules cm^{-2} s. It is noteworthy to point out that any single

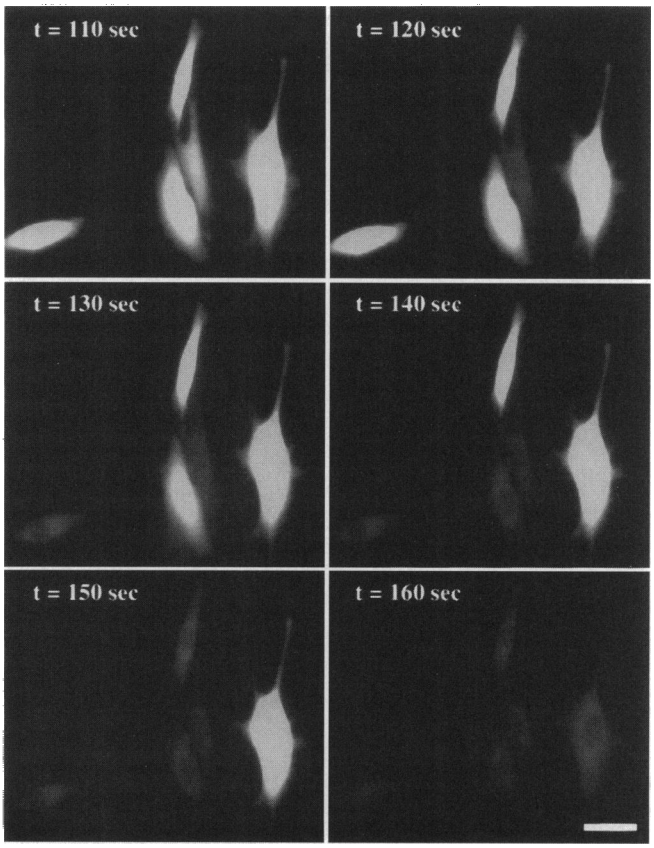

FIGURE 2 Micrographs of a representative dye leakage experiment from M21 cells. The experiment was performed at a laser power density of 200 mW cm^{-2} and SnCe6 concentration of 25 μM. The time points are shown on the micrographs. Scale bar represents 20 μm.

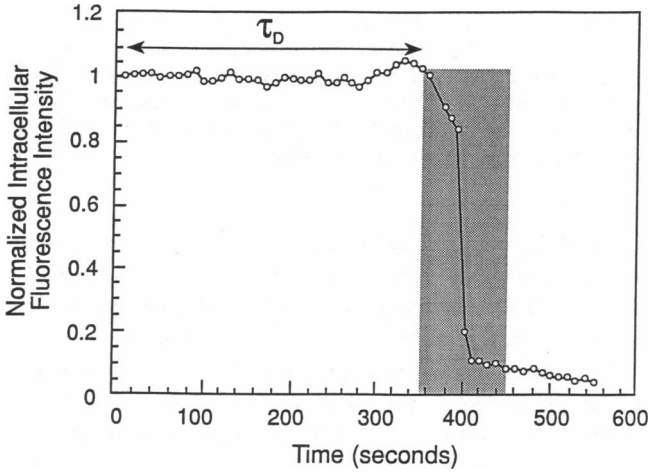

FIGURE 3 Normalized intracellular fluorescent intensity of a M21 cell as a function of time. The time lag before rupture is noted by the arrow associated with τ_D. The time constant associated with loss of dye from the cell τ_L is fit to the data in the shaded region.

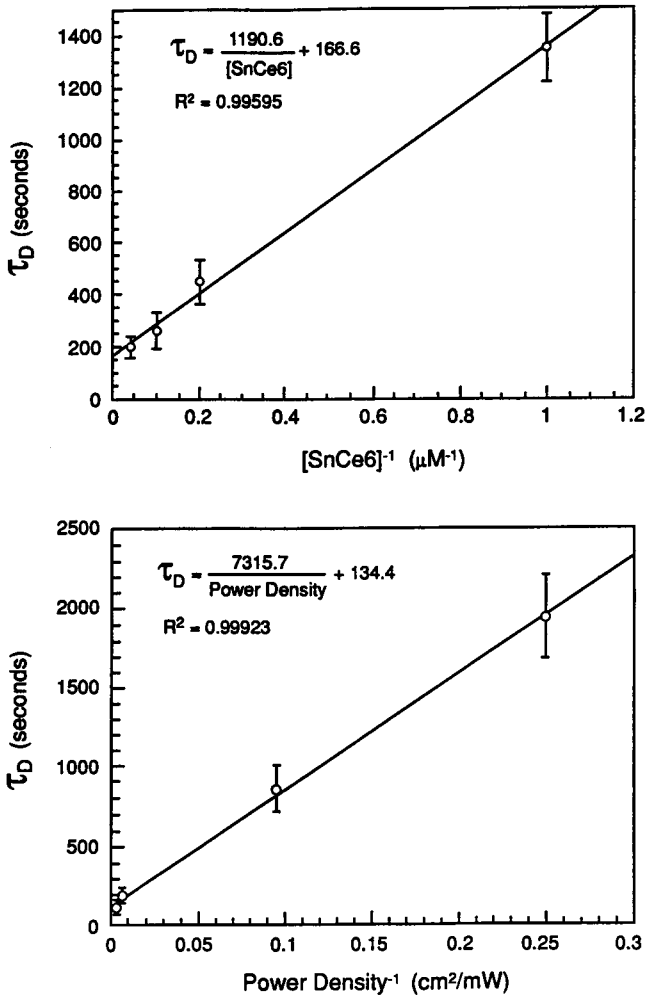

FIGURE 4 Lag time τ_D before membrane rupture as a function of (*top*) SnCe6 concentration (μM) at a constant laser power density of 150 mW cm^{-2}, and (*bottom*) laser power density (mW cm^{-2}) for a constant SnCe6 concentration of 25 μM. The data represent mean τ_D values from cell populations (~15 cells/experiment, 3–5 experiments/data point). Error bars represent the standard deviation from the mean.

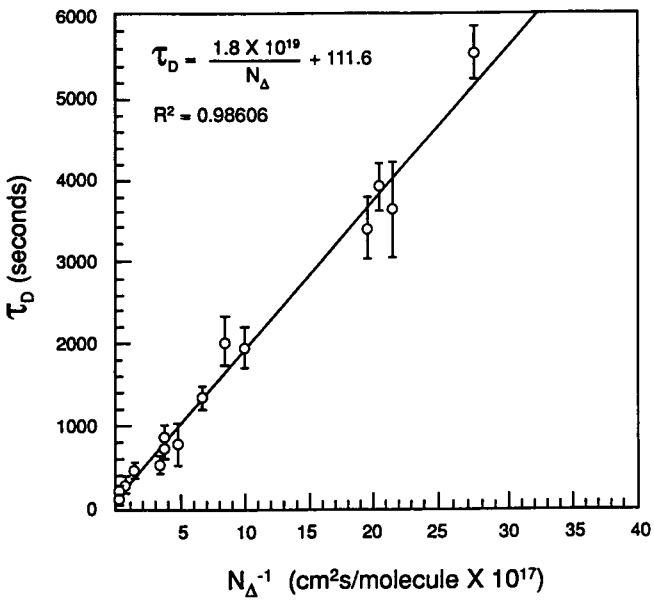

FIGURE 5 Lag time τ_D of membrane rupture as a function of inverse estimated singlet oxygen flux. The data represent mean values of τ_D from cell populations (~15 cells/experiment, 3–20 experiments/data point). Error bars represent the standard deviation from the mean.

value of N_Δ could be obtained by infinite different combinations of power density and PS concentration. These results clearly indicated that N_Δ was a key factor that dictated the lag period, τ_D, before sudden loss of cell membrane integrity.

The rate of calcein leakage out of M21 cells subsequent to the lag period τ_D was also determined for various photodamage conditions in order to obtain further information about the mechanism of cell lysis. A time constant characteristic of this leakage rate (τ_L) was determined for each cell by application of a simple mass balance for calcein at the time of rupture (see Eq. 3). τ_L represents the time at which 67% of the calcein had leaked out of the cell. The mean time constant for calcein leakage from cells in photolysis experiments was evaluated for various estimated singlet oxygen flux conditions ($N_\Delta = 6.0 \times 10^{17}$, 5.7×10^{16}, and 2.8×10^{16} molecules cm^{-2} s). The value of τ_L was independent of N_Δ with an average value for τ_L of 12 $\pm$ 1 s for these estimated singlet oxygen fluxes. These results suggested that the process of the sudden leakage of dye from cells was independent of photodamage conditions occurring at the surface of the cell. In fact, subsequent examination of individual cells with DIC optics (Fig. 6) at the onset of dye loss showed that the cell membrane was ruptured at a single point on the plasma membrane resulting in the sudden loss of dye from the cells. Further evidence for cell membrane rupture was obtained from the pattern of calcein leakage from individual cells as shown in Fig. 7. A characteristic pattern of leakage was observed in which the fluorescence appeared to burst out of the cell at a single point in the membrane. The fluorescence within the cell dissipated quickly through the apparent rupture site. Although this common pattern was observed in all of our experiments, the site of the rupture did not appear to be associated with any common membrane structure.

In the next series of experiments, the dynamics of targeted (i.e., ATPL) photolysis was compared with non-targeted (i. e., PDT) photolysis by employing an anti-ICAM immunoconjugate with a PS/MAb loading of 10:1. Cells were incubated with immunoconjugate for 5 min before laser irradiation. We compared populations of cells treated with different concentrations of PS (1, 5 and 25 μM SnCe6) with ATPL treated cells (with an immunoconjugate concentration of 10 nM). The laser power density was 150 mW cm^{-2} for all cell populations. Qualitatively, the ATPL treated cells were observed to responded the same as PS-treated cells (i.e., a time lag followed by cell membrane rupture). Furthermore, the τ_L values for ATPL treated cells were not significantly different than values obtained from PS treated cells. Fig. 8 shows the cumulative frequency of cellular membrane rupture as a function of irradiation time. As shown in Fig. 8, the ATPL treated cell curve most closely corresponds to cells

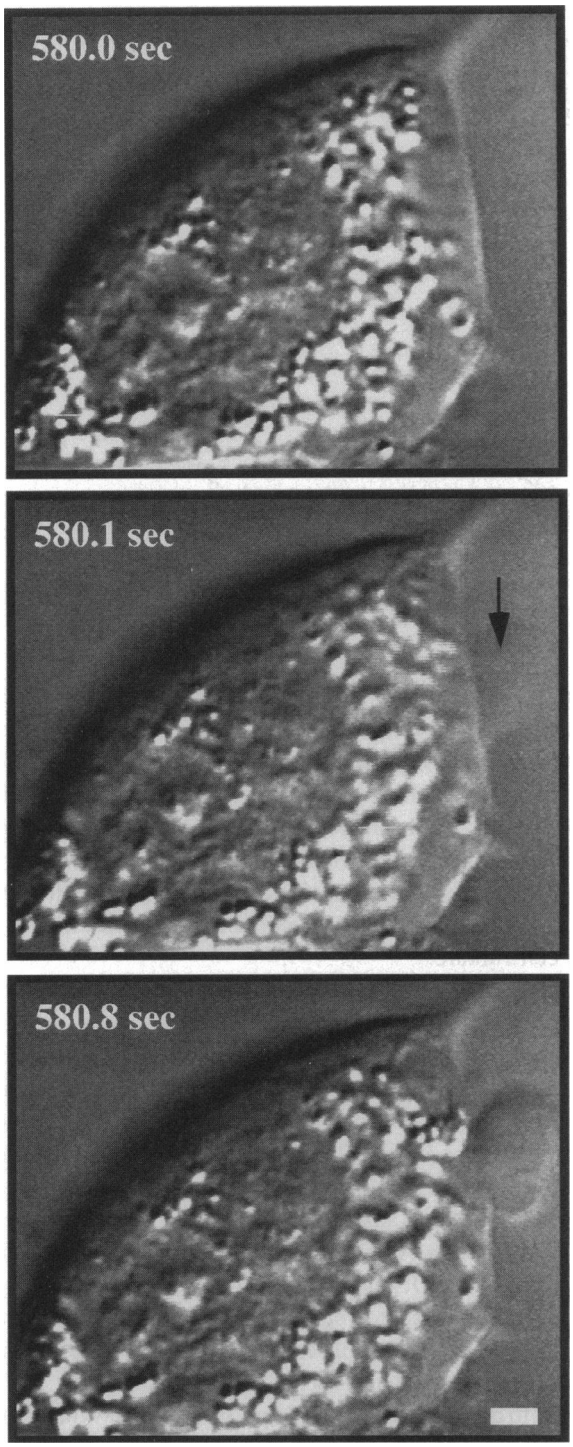

FIGURE 6 Micrograph of M21 cells in real time during photo-induced damage: Nomarsky DIC microscopy. Cells were laser irradiated at 40 mW cm^{-2} in the presence of 10 μM SnCe6. The corresponding times are shown on the micrographs. The arrow indicates the site of point rupture in the membrane. The scale bar represents 1 μm.

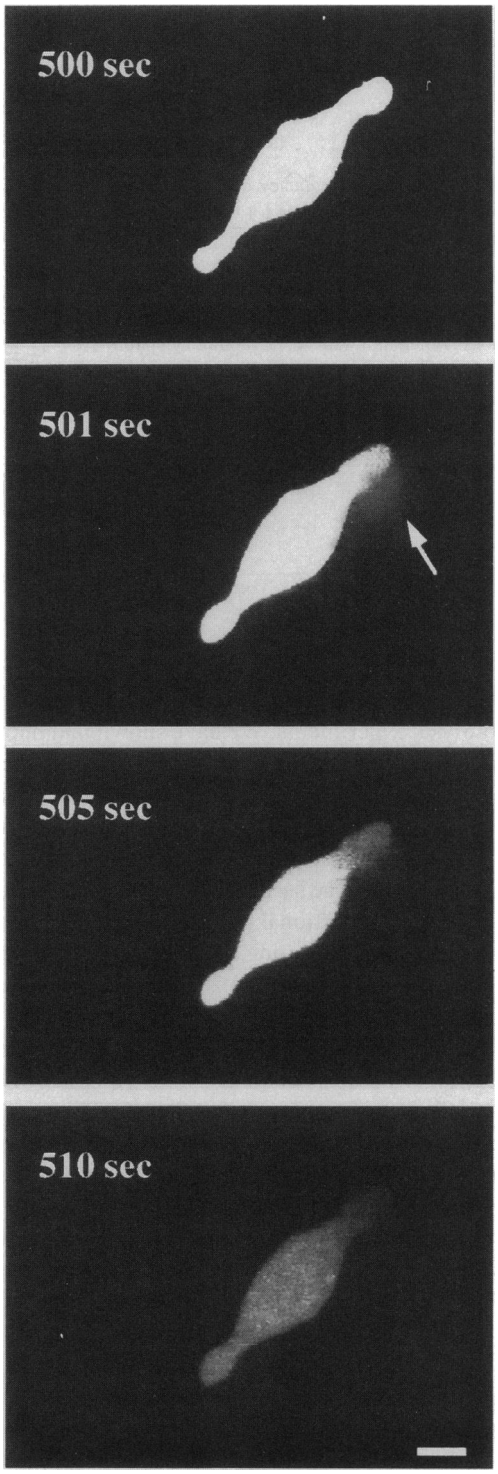

FIGURE 7 Micrograph of M21 cells in real time during photo-induced damage: Fluorescence microscopy. Cells were laser irradiated at 45 mW cm^{-2} in the presence of 10 μM SnCe6. The corresponding times are shown on the micrographs. The arrow indicates the site of point rupture in the membrane. The scale bar represents 5 μm.

treated with ~5 μM of free PS. Since the concentration of immunoconjugate was 10 nM (or ~100 nM PS concentration), the photodynamic effect afforded by ATPL is enhanced (approximately one order of magnitude).

DISCUSSION

We have developed a technique to examine in real time the dynamics of membrane rupture in single cells elicited by photodamage. This technique used a fluorescent membrane

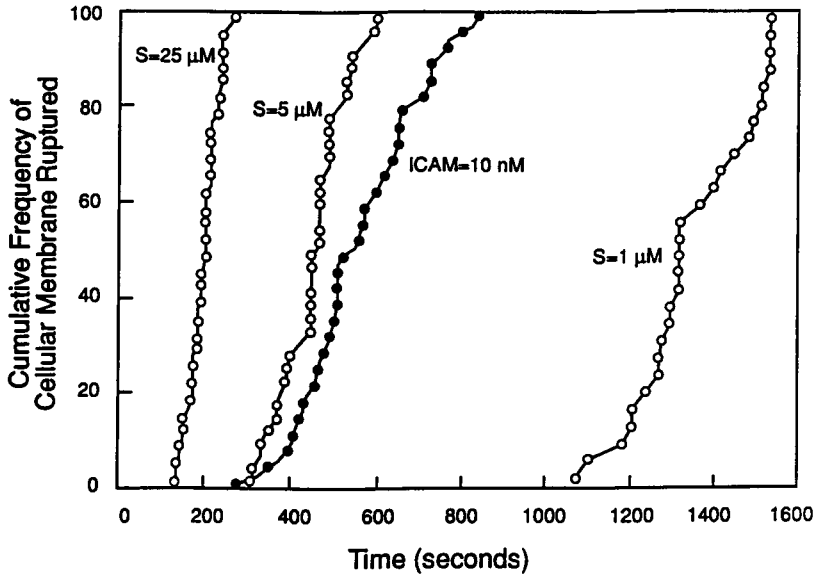

FIGURE 8 Cumulative frequency of cellular membrane rupture as a function of time for various PS concentration and a anti-ICAM immunoconjugate. Laser power density was 150 mW cm^{-2} for all cells treated. The ICAM immunoconjugate and free PS concentrations are shown on the figure. The data represent the time points at which individual cells rupture in a population. Each curve represents cell population ranging from 40 cells >400 cells (only 30 representative data points are shown per curve for clarity).

integrity probe (calcein) and quantitative microscopy to analyze photolysis experiments. We have shown that photodamage caused a sudden rupture of the plasma membrane which occurred after a time lag, τ_D, which directly correlated to irradiation power density and PS concentration. By using a kinetic/diffusional model, we estimated the singlet oxygen flux (N_Δ) delivered to the surface of irradiated cells and found it to be inversely proportional to τ_D. Upon examination of the kinetics of dye leakage during the rupture event, as characterized by a dye leakage time constant, τ_L, we found that the kinetics of leakage were independent of the estimated singlet oxygen flux levels. Additionally, we quantified the increase in efficiency (with respect to absolute amounts of PS required) obtained by use of targeted (i.e., ATPL) versus nontargeted (i.e., free PS) photodamage in eliciting cell rupture.

Cells were shown to respond to photodamage by a sudden rupture of their plasma membrane after a lag period during which the membrane appeared to be stable and impermeable to the vital dye, calcein. In all experiments, a time lag (τ_D) was noted before rupture. This characteristic delay period before cell rupture has been described in prior studies by Deziel, using erythrocyte ghosts (Deziel, 1981). Later reports utilizing the same erythrocyte ghost system but with different photosensitizing agents also noted a lag phase before the release of intracellular markers from a large population of cells (Girotti and Deziel, 1983). The present study, however, is the first to dynamically evaluate the lysis of single cells and to correlate the lag phase, τ_D with PS concentration and power density. Both power density and SnCe6 concentrations have been shown to vary inversely with τ_D. These correlations were expected since an increase in either power density or SnCe6 concentration should result in generation of more singlet oxygen and therefore lead to greater photodamage to the cell membrane. If this was the case, then a key factor in determining τ_D should be the flux of singlet oxygen to the surface of the cells. The singlet oxygen flux was calculated for a wide range of power densities and PS concentrations using a reaction/diffusion model. An inverse relation between τ_D and estimated singlet oxygen flux (N_Δ) has been demonstrated and this relation allows for the reduction of all experimental results in terms of N_Δ. Although this strong correlation between τ_D and N_Δ indicates that N_Δ is involved in cell membrane rupture, it does not give insight to the actual processes occurring in the membrane during irradiation before cell rupture.

Examination of the kinetics of dye leakage during the rupture process could give important information on how the rupture occurs. Analysis of the dye leakage time constant τ_L, indicated that once initiated, cells ruptured at a rate independent of flux conditions. The average time for 67% of dye leakage was approximately 12 s. A mass balance over the cell for calcein leakage revealed that this time constant corresponded to a defect size on the order of 73 nm in diameter. This estimate is an order of magnitude larger than the defect size estimate by Deziel and Girrotti based upon the leakage of markers from photolysed erythrocyte ghosts (Deziel and Girrotti, 1982). A plausible explanation for the disagreement between these estimates is that erythrocyte ghosts are not subject to any colloidal osmotic pressure effects which could increase the net leakage rate of calcein leakage in a intact living cell. This increase in dye leakage would result in a lesion size overestimation since the mass balance utilized only considers passive diffusion of dye out of the ruptured cell rather than considering contributions from pressure induced dye convection. In addition, our analysis is based upon the assumption that the lesion size is invariant with time. However, close examination of our video suggests that the initial rupture results in an ongoing and fast (<2 s) disruption of the plasma membrane surrounding the original lesion which likely enlarges the net lesion size available for dye leakage. The lesion size estimate from our analysis therefore

would be an overestimate since it would be based upon leakage rates from cells predominately during the later phase of the dye loss.

Since the dose of singlet oxygen delivered is proportional to both τ_D and the estimated N_Δ (i.e., dose = $N_\Delta \times \tau_D \times S_T$), the anticipated relationship between N_Δ^{-1} and τ_D should be linear with a y intercept of 0 (corresponding to infinite N_Δ). While this relationship shown in Fig. 5 is clearly linear, it shows a y intercept of 112 ± 73 s. This value is an order of magnitude larger than the mean time for calcein to leak out of ruptured cells as noted above (i.e., τ_L = 12 s) indicating that passive diffusion of calcein alone can not account for this additional delay time. The presence of a y intercept suggests that even at the highest estimated singlet oxygen flux conditions (corresponding to the highest photodamage rates) there is a significant delay to the onset of cell rupture.

One explanation which could account for this extra delay time may be that rupture is conditional upon another "intrinsic" membrane process apart from the photodamage process. A similar mechanism has previously been proposed for γ particle irradiation induced peroxidation of membrane lipids (Canaday et al., 1994). While their peroxidation mechanism is different than that occurring in our study, our results (i.e., membrane rupture following a time lag) were similar to their findings. Presumably, after a sufficient amount of photodamage has accumulated within the membrane, a reorganization of the cell membrane components may occur leading to the onset of membrane rupture. This reorganization of the membrane could be an aggregation process, possibly of "damaged" lipids. This aggregation process would be limited by diffusional constraints within the membrane which could account for a delay in rupture onset. If operative, this diffusional constraint should be most apparent at the highest flux conditions. Closer examination of the highest four estimated flux conditions with respect to τ_D (corresponding to flux levels from 7×10^{16} to 9.4×10^{17} molecules cm^{-2}), and plotting each as in Fig. 5, yields a y intercept value of 113 ± 13 s (figure not shown). Given the significance of this y intercept value, the additional contribution to τ_D at high N_Δ conditions likely represents a regime which is diffusionally controlled. Conversely, we expect that at low estimated flux conditions, the effect of this diffusional constraint would be minimal, since the τ_D values for these flux conditions are $\gg$112 s. Examination of the lowest 14 estimated flux conditions with respect to τ_D (corresponding to flux levels from 3.6×10^{15} to 2×10^{16} molecules cm^{-2}), and plotting each as in Fig. 5, yields a y intercept of 61 ± 135 s (figure not shown). As expected, low flux regime data suggest that there is no significant increase in τ_D that may arise from a diffusionally controlled process as evidenced by the small y intercept (which is not significantly different from 0). Thus, these results suggest that there is a distinct contribution to τ_D which may depend upon a membrane related diffusion process.

Among the major advantages of the approach developed in this study is the ability to quantitatively test the efficiency of various targeting modalities. To this end, we assessed the relative efficiency of MAb-conjugated PS to that of free PS in solution. Although the kinetics of calcein leakage following membrane rupture was identical in both cases, (PDT vs. ATPL), the concentration of immunoconjugate required to rupture cells was two orders of magnitude smaller than corresponding free PS concentrations (10 nm versus ~3.3 μM, Fig. 8). This result clearly supports the hypothesis that the efficiency of targeted photodamage can be greatly improved over that of non-targeted modalities. In addition, since the ICAM immunoconjugate localizes the PS to the surface of the cell membrane, the assumption that the cell membrane is the principle target of photodamage is further supported. Given the similarity of rupture phenomenon using either free PS or immunoconjugate, the assumption that free PS induced photodamage is also associated primarily with the cell membrane is also supported.

In this study, we examined the phenomenological behavior of photodamaged cells. However, by appropriate choice of probe dyes, information pertaining to the specific mechanism of action may be obtained. Moreover, the system is also capable of changing temperature dynamically, which would yield values of the activation energies enabling a more mechanistic understanding of the photodamage process. Current and future studies will utilize these features of the experimental system in order to further probe the mechanism of action.

In summary, we have developed a quantitative approach for examining plasma membrane damage resulting from photochemical action of SnCe6. Microscopic examination of the photolysis process indicated that cell membrane ruptured at a single point. The time delay measured before plasma membrane rupture appears to incorporate two distinct contributions: 1) the time required to produce a minimum number of damage sites, and 2) the time required for membrane surface re-organization. We are currently developing a phenomenological model which incorporates both of these phenomenon that could help to elucidate the mechanism(s) involved in the rupture phenomenon described here as well as suggest further studies to help understand the photodamage process in general.

We thank William Holmes for technical assistance with image analysis and Drs. L. Strong and S. Reicken for critical reviews.

This work was supported by grant T32 GM08339 from the National Institutes of Health and by the Shriners Hospitals for Children (SHC).

REFERENCES

Brault, D., C. Vever-Bizet, M. Rougee, and R. Bensasson. 1988. Photophysical properties of a chlorin, a potent sensitizer for photochemotherapy. *Photochem. Photobiol.* 47:151–154.

Canaday, D., P. Li, R. Weichselbaum, R. D. Astumian, and R. C. Lee. 1994. Membrane permeability changes in gamma-irradiated muscle cells. *Ann. N.Y. Acad. Sci.* 720:153–159.

Comporti, M. 1989. Three models of free radical-induced cell injury. *Chem. Biol. Interact.* 72:1–56.

Deziel, M. R. 1981. The Photodynamic Action of Bilirubin on Biological Membranes. Doctoral Dissertation, Medical College of Wisconsin, Wisconsin.

Deziel, M. R., and A. W. Girotti. 1982. Lysis of resealed erythrocyte ghosts by photoactivated tetropyrroles: estimation of photolesion dimensions. *Int. J. Biochem.* 14:263–266.

Dougherty, T. J. 1993. Yearly review: photodynamic therapy. *Photochem. Photobiol.* 58:895–900.

Fingar, V. H., T. J. Wieman, S. A. Wiehle, and P. B. Cerrito. 1992. The role of microvascular damage in photodynamic therapy: the effect of treatment on vessel constriction, permeability, and leukocyte adhesion. *Cancer Res.* 52:4914–4921.

Girotti, A. W. 1979. Protoporphyrin-sensitized photodamage in isolated membranes of human erythrocytes. *Biochemistry.* 18:4403–4411.

Girotti, A. W. 1990. Photodynamic lipid peroxidation in biological systems. *Photochem. Photobiol.* 51:497–509.

Girotti, A. W., and M. R. Deziel. 1983. Photodynamic action of protoporphyrin on resealed erythrocyte membranes: mechanism of release of trapped markers. *Adv. Exp. Med. Biol.* 160:213–225.

Gollnick, A. W. 1968. Type II photooxygenation reactions in solution. *Adv. Photochem.* 6:1–122

Gomer, C. J. 1991. Preclinical examination of first and second generation photosensitizers used in photodynamic therapy. *Photochem. Photobiol.* 54:1093–1107.

Hartman, P. E., W. J. Dixon, T. A. Dahl, and M. E. Daub. 1988. Multiple modes of photodynamic action by cercosporin. *Photochem. Photobiol.* 47:699–703.

Jiang, F. N., D. J. Liu, H. Neyndorff, M. Chester, S. Jiang, and J. G. Levy. 1991. Photodynamic killing of human squamous cell carcinoma cells using a monoclonal antibody-photosensitizer conjugate. *J. Natl. Cancer Inst.* 83:1218–1225.

Lindig, B. A., and M. A. J. Rodgers. 1981. Rate parameters for the quenching of singlet oxygen by water-soluble and lipid-soluble substrates in aqueous and micellar systems. *Photochem. Photobiol.* 33:627–634.

Lu, X. M., A. J. Fischman, E. Stevens, T. T. Lee, L. Strong, R. G. Tompkins, and M. L. Yarmush. 1992. Sn-chlorin e6 antibacterial immunoconjugates: an in vitro and in vivo analysis. *J. Immunol. Methods.* 156:85–99.

Matthews, W., J. Cook, M. J. B., R. R. Perry, S. Evans, and H. I. Pass. 1989. In vitro photodynamic therapy of human lung cancer: investigation of dose-rate effects. *Cancer Res.* 49:1718–1721.

Oseroff, A. R., D. Ohuoha, T. Hasan, J. C. Bommer, and M. L. Yarmush. 1986. Antibody-targeted photolysis: selective photodestruction of human T-cell leukemia cells using monoclonal antibody-chlorin e_6 conjugates. *Proc. Natl. Acad. Sci. USA.* 83:8744–8748.

Potter, W. R., T. S. Mang, and T. J. Dougherty. 1987. The theory of photodynamic therapy dosimetry: consequences of photo-destruction of sensitizer. *Photochem. Photobiol.* 46:97–101.

Rakestraw, S. L. 1989 Antibody-Targeted Photolysis. Doctoral Dissertation, Massachusetts Institute of Technology, Cambridge, Massachusetts.

Rakestraw, S. L., W. E. Ford, R. G. Tompkins, M. A. J. Rodgers, W. P. Thorpe, and M. L. Yarmush. 1992. Antibody-targeted photolysis: in vitro immunological, photophysical, and cytotoxic properties of monoclonal antibody-dextran-Sn(IV) chlorin e_6 immunoconjugates. *Biotechnol. Prog.* 8:30–39.

Rodgers, M. A. J., and P. T. Snowden. 1982. Lifetime of singlet oxygen in liquid water as determined by time resolved infrared luminescence measurements. *J. Am. Chem. Soc.* 104:5541–5543.

von Asmuth, E. J., E. F. Smeets, L. A. Ginsel, J. J. Onderwater, J. F. Leeuwenberg, and W. A. Buurman. 1992. Evidence of endocytosis of E-selectin in human endothelial cells. *Eur. J. Immunol.* 22: 2519–2526.

Yarmush, M. L., W. P. Thorpe, L. Strong, S. L. Rakestraw, M. Toner, and R. G. Tompkins. 1993. Antibody-targeted photolysis. *In* Critical Reviews in Therapeutic Drug Carrier Systems. CRC Press, Boca Raton, FL.